Available online at www.sciencedirect.com
SCIENCE DIRECT
Polymer 47 (2006) 5871–5879
polymer
www.elsevier.com/locate/polymer

Effect of molecular and processing parameters on the flow-induced crystallization of poly-1-butene. Part 1: Kinetics and morphology

Jimmy Baert, Peter Van Puyvelde*

K.U. Leuven, Department of Chemical Engineering, W. de Croylaan 46, B-3001 Leuven, Belgium

Received 9 January 2006; received in revised form 30 May 2006; accepted 6 June 2006
Available online 30 June 2006

Abstract

In this work the effect of molecular parameters (molecular weight (M_W), molecular weight distribution (MWD)) and processing conditions (crystallization temperature, flow conditions) on the isothermal crystallization behavior of three isotactic poly-1-butene (iPB) samples is investigated by means of rheo-optical techniques. The emphasis in this paper will be on the kinetics and the resulting morphology.

Turbidity measurements show a strong effect of M_W and the degree of undercooling on the flow-induced crystallization (FIC), whereas the effect of MWD is not quite clear. Scaling relations, proposed in literature, that are based on polymer chain relaxation were found to predict correctly the dependence of FIC, at least when samples of similar MWD are considered. A mastercurve is presented combining effects of M_W, shear strain, shear rate and temperature.

Optical microscopy observations provide information on the quiescent growth rate and the morphology of the crystallites. The effect of the different parameters on the observed transition from an isotropic morphology at low shear rates to a rod-like crystalline structure at high shear rates, could again be explained in terms of polymer chain relaxation.

Keywords: Flow-induced crystallization; Kinetics; Morphology

1. Introduction

During processing, molten polymers are unavoidably subjected to strong deformations and complex thermal histories. Semicrystalline materials will crystallize after or even during flow. The properties of the final product will hence be affected by both the thermal and the mechanical history that the polymer experiences in the molten state (e.g. [1]).

To improve our understanding of the crystallization process from a fundamental point of view, it has been proven useful to separate the thermal and flow effects. Several researchers have studied flow-induced crystallization (FIC) in well-defined flows and under isothermal conditions [2,3]. The short-time shearing protocol, introduced by Janeschitz-Kriegl and coworkers [4], enables separation of flow, nucleation and growth phenomena. It has been used to study flow-enhanced crystallization at high shear rates although the applied flow field was not a simple shear flow [4–6]. In the present work, separation of flow, nucleation and growth will be used as well, but in simple shear flow and at relatively mild flow intensities.

The application of shear flow to an undercooled polymer melt is known to enhance the crystallization process. The extent of this enhancement depends on many factors, such as the processing parameters and the molecular properties of the polymer. Evidence of the effects of M_W on the crystallization rate under flow can be found in the literature. Jay et al. [7] and Duplay et al. [8] performed fiber-pulling experiments on a long series of isotactic polypropylenes (iPP) of varying M_W. The results showed that, for a specific shear rate, the global crystallization speed increases exponentially with increasing M_W.

* Corresponding author. Tel.: +32 16 322357; fax: +32 16 322991.
E-mail address: peter.vanpuyvelde@cit.kuleuven.be (P. Van Puyvelde).

0032-3861/$ - see front matter © 2006 Elsevier Ltd. All rights reserved.
doi:10.1016/j.polymer.2006.06.009

Vleeshouwers and Meijer [9] performed rheological flow-induced crystallization experiments on iPP samples of different M_W and MWD. They found that for a specific shear rate, the increase in crystallization kinetics is larger for high M_W samples. Jerschow and Janeschitz-Kriegl [5] carried out simulated injection molding experiments on several commercial iPP samples. The results showed that long polymer molecules are predominantly responsible for the formation of highly oriented surface layers due to shear treatment. Somani et al. [10] used small angle X-ray scattering to characterize the crystallization rate of iPP after an isothermal step shear flow. The authors suggested that in polydisperse samples only polymer chains above a critical M_W contribute to the formation of oriented structures. Bove and Nobile [11,12] used rheological measurements to follow the crystallization kinetics of two iPBs with different M_W, both under quiescent conditions and after imposing a shear flow. In agreement with Jay et al. [7] and Somani et al. [10], they found that the material with the highest M_W is most sensitive to shear flow. Moreover, they stated that for a specific shear strain a critical shear rate is required to effect crystallization kinetics. Coppola et al. [13] found a more pronounced sensitivity of the dimensionless crystallization time to flow intensity at higher crystallization temperatures (closer to the thermodynamic melting point).

Despite the above reported experimental efforts, a more quantitative assessment of the effects of different parameters on FIC is rare. Recently, the effects of M_W and MWD on flow-induced crystallization of iPB were quantified by Acierno et al. [14,15] and Hadinata et al. [16]. Acierno et al. [14,15] carried out both rheological and optical shear flow experiments on a set of iPB samples. They observed a strong effect of M_W on the flow-induced crystallization kinetics and it was shown that such an effect could be cast in terms of molecular parameters. The M_W scaling was also found to explain qualitatively the observed transition from a low-shear rate isotropic morphology to a high-shear rate rod-like crystalline structure. Hadinata et al. [16] performed rheological shear flow experiments on a similar set of iPB samples. They showed that, in the range of low shear rates ($<0.3\ s^{-1}$), the results yield a temperature-invariant representation by scaling the y-axis and the x-axis in a graph of the crystallization onset time versus shear rate. This curve has a plateau-and-slope shape that fits into a three-parameter cross function. Furthermore, they observed that the location and the shape of the curve depend on the M_W and the MWD.

In this paper, the effects of several relevant processing parameters on the kinetics and morphology of the flow-induced crystallization of various iPB samples are discussed.

2. Materials and methods

2.1. Materials

The three iPB samples used in this work were provided by Basell Polyolefines in the form of pellets, without nucleating agents. The molecular parameters as obtained from GPC measurements by Basell are described in Table 1. The index of tacticity was the same for all M_W's investigated (98.8%).

Table 1
Molecular parameters of the iPB samples

Type	PB0800	PB0400	BR200
M_w [g/mol]	85 000	176 000	762 000
M_w/M_n	5.1	5.7	19.6

Disc-shaped samples of iPB were prepared from the as-received pellets by molding at 200 °C and 100 bar for 4 min in a Collin laboratory press. In the rheometer and optical cell, samples were always annealed at 200 °C for 10 min to erase the thermal and flow history. A sufficiently high annealing temperature and annealing time have been chosen based on experiments with BR200, which is the iPB sample having the highest M_W. Dynamic measurements during heating and cooling of the iPB samples (both at a rate of 10 °C/min) showed that only at temperatures above 160 °C BR200 is completely melted. This is illustrated in Fig. 1 in which the complex viscosity is shown as a function of temperature during both a heating cycle and a cooling cycle. From this graph, it is seen that above a temperature of 160 °C, no rheological hysteresis can be observed. Hence, above this temperature, the material is in the molten state. Hadinata et al. [16] showed that annealing at 160 °C for 5 min still resulted in residual nuclei, hence it was decided to heat the iPBs sufficiently in order to erase the thermomechanical properties.

2.2. Methods

The linear viscoelastic characterization of the three polymers was performed on a stress controlled rotational rheometer (Rheometrics DSR, Rheometrics Inc.). This rheometer was equipped with parallel plate fixtures (plate diameter 25 mm, gap thickness 1 mm). Measurements were carried out under a dry nitrogen atmosphere to minimize polymer degradation. Experiments were performed in the temperature range 160–200 °C.

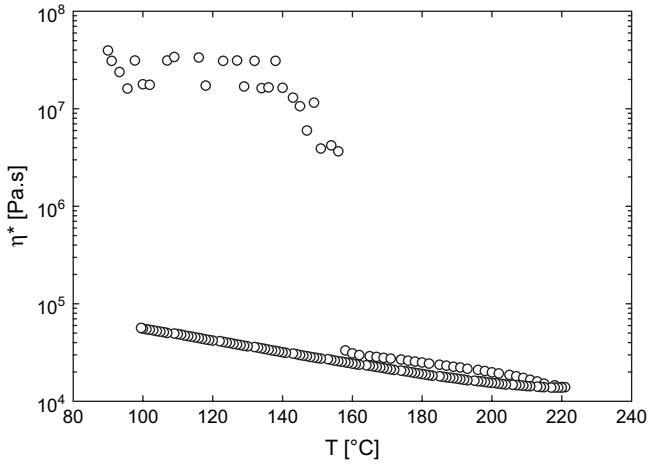

Fig. 1. Rheological hysteresis during heating and cooling of BR200 (frequency = 1 rad/s).

The development of crystallinity was followed by turbidity measurements in a Linkam optical cell (CSS 450, Linkam Scientific Instruments Ltd) equipped with glass parallel plates. A typical sample thickness of 0.4 mm was used. The optical train consisted of a linearly polarized laser light source (10 mW He–Ne, wavelength 623.8 nm), a polarizer and a photodiode. The mechanical design and electronic control of the Linkam shear cell allowed to precisely control the shear field and the thermal history of the samples. In all experiments the step shear mode was selected, which allows the shear parameters (shear rate $\dot{\gamma}$ and shear strain γ) to be varied independently.

The flow-induced isothermal crystallization studies followed the experimental protocol shown in Fig. 2: pre-heating of the sample to 200 °C, annealing at 200 °C for 10 min to eliminate all possible residual structures and cooling at a rate of 10 °C/min down to the desired crystallization temperature T_c. Zero time scale was assigned to the instant at which the crystallization temperature was reached. Shear flow was then applied at different shear rates, $\dot{\gamma}$, and for different shearing times, t_s, with the constraint of a constant applied shear strain: $\gamma = \dot{\gamma} t_s$. After cessation of shear flow, the samples crystallize isothermally and the intensity of transmitted light was then measured as a function of time. The measured intensity was normalized as follows:

$$I(t) = \frac{I_m(t) - I_{min}}{I_0 - I_{min}} \quad (1)$$

where $I_m(t)$ is the measured intensity, I_0 the intensity at $t = 0$ and I_{min} the minimum intensity over the experimental time range.

The turbidity measurements were complemented by direct optical microscopy observations. To this end the sample was placed in the Linkam optical cell and observed under a polarizing microscope (Laborlux 12 Pol S, Leitz). The microscope was equipped with a camera (C4742-95, Hamamatsu Photonics) and different magnification objectives. Microscope images were directly digitized by means of a frame grabber (HiPic 6.4.0, Hamamatsu Photonics). Quantitative analysis of the digital images was carried out using suitable software (Scion Image, Scion Corp.). The same experimental protocol was used as for the turbidity measurements.

For the iPBs, the turbidity measurements and the optical microscopy observations were carried out at three different crystallization temperatures, namely, 93 °C, 98 °C and 103 °C. The choice of the three test temperatures was dictated by two important constraints. On the one hand, temperatures were chosen so as to determine measurable characteristic crystallization times. In fact, too high temperatures (close to the thermodynamic melting temperature T_m^0) resulted in very low crystallization rates, whereas too low temperatures caused an essentially instantaneous crystallization. In both cases, the measurement of the characteristic time becomes impossible, or at best unreliable. On the other hand, the three temperatures were chosen in order to determine the largest possible difference in characteristic time, in order to guarantee the highest amplification of the temperature effect.

3. Results and discussion

3.1. Rheology

The complex viscosity as a function of frequency is shown in Fig. 3. Time–temperature superposition to the reference temperature of 180 °C collapses the data into a single mastercurve for each M_W. Only the horizontal shift procedure was adopted.

The iPB samples show the typical linear viscoelastic behavior of a modestly entangled polymer melt. For PB0800 and PB0400 the terminal region is well represented, as confirmed

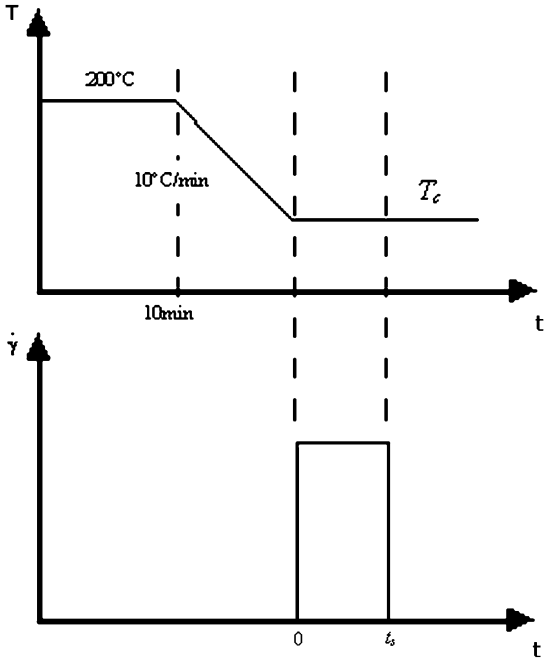

Fig. 2. Schematics of the temperature and shear conditions as a function of time.

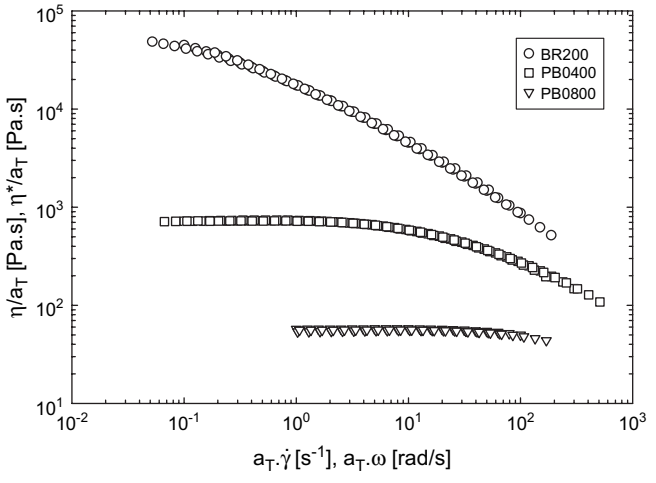

Fig. 3. Complex viscosity mastercurves of the three iPB samples at the reference temperature of 180 °C.

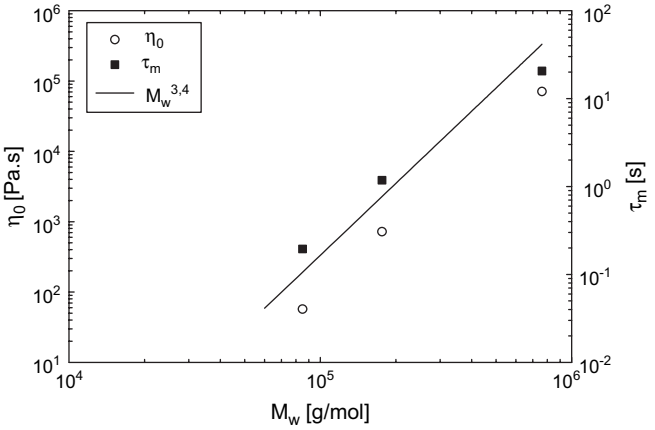

Fig. 4. Zero-shear rate viscosity and average relaxation time at 180 °C as a function of the weight average molecular weight.

by the low frequency plateau of the complex viscosity. On the other hand, BR200 does not show the typical asymptotic behavior within the measured frequency region. The broad transition to the terminal region is caused by the larger MWD. The zero-shear rate viscosity, η_0, is a strong function of M_W, and the crossover to the shear thinning behavior occurs at lower and lower shear rates as the M_W increases. The effect of M_W on the zero-shear rate viscosity is shown in Fig. 4. The data are well fitted by a power law:

$$\eta_0 \div M_w^{3.4} \tag{2}$$

which is in good agreement with predictions for entangled polymer melts [17].

The shift factors (not reported here) are found to obey an Arrhenius relationship, as expected for temperatures well above the polymer glass transition. From a linear regression of the shift factor data, the activation energy for each polymer can be extracted. The activation energies are reported in Table 2.

The shift factors and the corresponding activation energies can then be used to relate the effects of flow on the crystallization kinetics. According to the scaling behavior proposed by Acierno et al. [15], based on the framework of the widely accepted reptation theory [18], the effect of flow on chain orientation, and therefore on flow-induced crystallization, can be put in dimensionless form by defining a Deborah number for the system as:

$$De = \dot{\gamma}\tau_d \tag{3}$$

with τ_d the relaxation or disengagement time. Whereas Acierno et al. [15] used the maximum relaxation time of the polymer system, τ_{max}, as a characteristic relaxation time, we used the average value over the relaxation spectrum $H(\tau)$, τ_m. The latter can be calculated from G' and G'', obtained from viscoelastic measurements, using the software NLREG (non-linear regularization) (Version Rheology 2.0, Freiburg Materials Research Center). As shown in Fig. 4 the average relaxation time increases with M_W as expected from the following relationship [17]:

$$\tau_m \div M_w^{3.4} \tag{4}$$

The average relaxation time of the three iPB samples at 103 °C, 98 °C and 93 °C has been estimated from the master-curves at 180 °C, followed by a time–temperature shift to the desired temperatures, where use of the activation energies (reported in Table 2) has been made.

Table 2
Activation energies and average relaxation times at 180 °C for the three iPB samples

Type	PB0800	PB0400	BR200
E [kJ/mol]	41	47.2	54.7
τ_m [s]	0.195	1.18	20.6

3.2. Rheo-optics

3.2.1. Crystallization kinetics

Fig. 5 shows a typical time-evolution of the normalized light intensity, I, during the crystallization of PB0400 at a temperature of 98 °C. In the quiescent experiment the intensity is almost constant up to times of the order of 10^3 s. During this time the polymer remains essentially in the state of the undercooled melt. As crystallization sets in, the nucleation and subsequent growth of the crystallites generate a strong and relatively fast increase of the sample turbidity, which corresponds to a reduction of I. At later stages, a low value of the transmitted light intensity, corresponding to the final semi-crystalline state, is eventually reached.

In order to characterize qualitatively the crystallization kinetics a "turbidity half-time", $t_{1/2}$, defined as the time where the transmitted intensity has decreased to 50% of its initial value, is used. It should be stressed that the choice of $t_{1/2}$ to characterize the crystallization kinetics is arbitrary but it provides a quick means of assessing the crystallization kinetics.

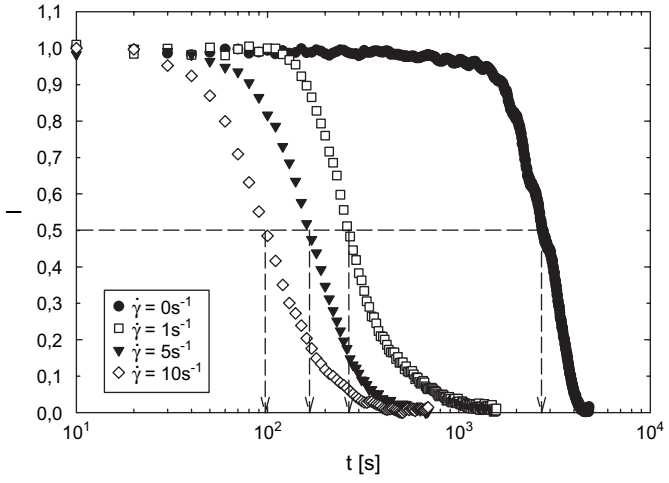

Fig. 5. Transmitted light intensity as a function of time for PB0400 at 98 °C under different flow conditions having constant shear strain $\gamma = 100$. Arrows indicate the turbidity half-time $t_{1/2}$.

The effects of flow on the crystallization kinetics can be further clarified by defining a dimensionless crystallization time, Θ, as the turbidity half-time at a given shear rate, $t_{1/2,\dot{\gamma}}$, divided by the corresponding turbidity half-time under quiescent conditions, $t_{1/2,q}$:

$$\Theta = \frac{t_{1/2,\dot{\gamma}}}{t_{1/2,q}} \tag{5}$$

Obviously, $\Theta = 1$ in the absence of flow, whereas $\Theta \leq 1$ under flow conditions.

The dimensionless crystallization time Θ is plotted as a function of shear rate in Fig. 6. Due to the choice of a log scale for the shear rate axis, the experimental points corresponding to quiescent conditions ($\dot{\gamma} = 0$, $\Theta = 1$) cannot be plotted. For clarity these points are displayed at a shear rate of 0.001 s^{-1}.

Fig. 6 clearly shows that the application of a shear flow significantly accelerates the crystallization kinetics, as reflected by the decreasing turbidity half-times with increasing shear rate. By increasing the M_W, the deviation from quiescent crystallization takes place at lower shear rates. Furthermore, an increase in M_W determines a larger increase of the flow-induced crystallization kinetics under the same shear rate. The same trends have been observed using a total shear strain of 10.

Fig. 7 shows the dimensionless crystallization time as a function of the Deborah number, $De = \dot{\gamma}\tau_m$. It can be observed that, with good approximation, for all M_W's the deviation from the quiescent condition takes place for values of $De > 1$, in agreement with the scaling behavior proposed by Acierno et al. [15]. The data for PB0400 and PB0800 fall on the same mastercurve. The data for BR200 deviate from it, which is most likely caused by the broader MWD. Moreover, for BR200 at 98 °C and a total shear strain of 100, there is already an influence of crystallization during flow.

From Fig. 7 we conclude that for relatively monodisperse samples, the effect of M_W on the crystallization kinetics can be scaled by means of an average relaxation time.

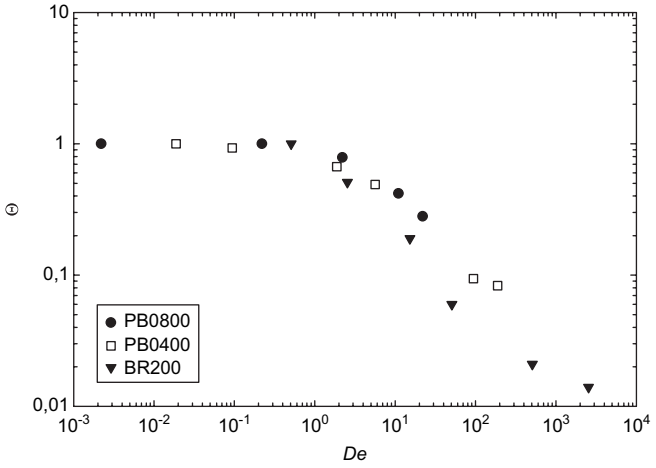

Fig. 7. Dimensionless crystallization time as a function of the Deborah number for the different molecular weight samples ($T_c = 98$ °C, $\gamma = 10$).

Not only the shear rate $\dot{\gamma}$ is of importance, the total shear strain $\gamma = \dot{\gamma}t_s$ (which for a constant shear rate is equivalent to the shearing time) also affects the polymer orientation and thus the crystallization time, as observed by Bove and Nobile [12]. These authors stated that both shear rate and shear strain are critical factors to form stable nuclei for the crystallization process from the flow oriented polymer chains. Fig. 8 shows that for a constant shear rate, a higher shear strain results in a larger increase in the crystallization kinetics. For low shear rates, the effect of shear strain (or shear time) is limited. The effect increases with flow intensity but much slower than the effect of shear rate itself. These results can be explained as followed: for small shear strains, even at high shear rates, the orientation and ordering of the polymer chains are insufficient to form nuclei. At low shear rates, even for large shear strains, the chains have sufficient time to relax and no stable nuclei are formed.

From Fig. 8 it seems that for a shear strain of 10 the effect of shear rate saturates, whereas for a shear strain of 100 this is not the case. To our knowledge such a plateau effect has not

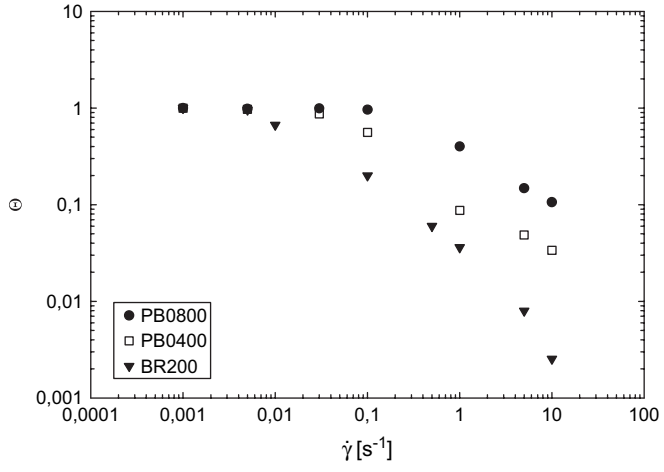

Fig. 6. Dimensionless crystallization time as a function of shear rate for the different molecular weight samples ($T_c = 98$ °C, $\gamma = 100$).

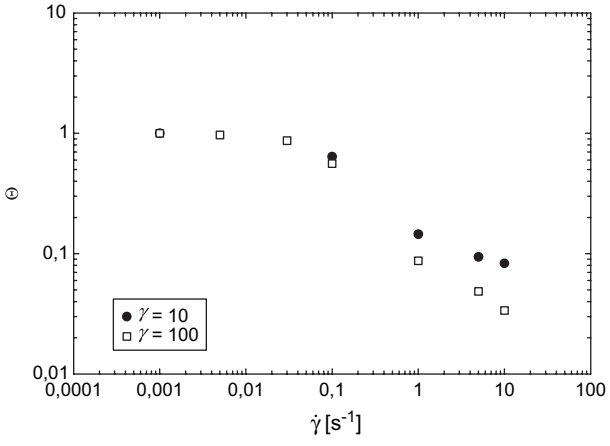

Fig. 8. Dimensionless crystallization time as a function of the shear rate for PB0400 at 98 °C and two different shear strains.

yet been described in literature. A possible explanation could be that for low shear times the Linkam optical cell fails in subjecting the polymer melt to a well evolved flow field. More experiments are necessary to clarify this. For the moment, this effect hampers the attempt to scale out the effect of the shear strain on the crystallization time and to obtain a strain-independent mastercurve.

Another parameter that strongly affects flow-induced crystallization is the crystallization temperature. In Fig. 9 (top) the experimentally obtained turbidity half-times of PB0400 for a shear strain of 100 are plotted as a function of shear rate. At higher crystallization temperatures, closer to the thermodynamic melting point, the crystallization times are clearly larger.

Again, for the different crystallization temperatures, the turbidity half-times under quiescent conditions are used to normalize the turbidity half-times under shear. This results in Fig. 9 (bottom) in which for PB0400 the dimensionless crystallization times Θ are plotted as a function of shear rate.

A more pronounced sensitivity of the dimensionless crystallization time to flow intensity is found at the higher crystallization temperatures. In other words, the slower the crystallization in quiescent conditions, the more pronounced is the relative effect of flow. This fact was also observed by Coppola et al. [13] who explained it in terms of polymer chain orientation. As the temperature increases, both the orientational effect of flow and the quiescent crystallization kinetics are depressed. The latter, however, is much more sensitive to temperature. Furthermore, while the intrinsic crystallization rate (i.e. in the absence of flow) tends to zero as the temperature approaches the thermodynamic melting point, the flow-induced orientation effect of flow survives at any temperature. As a consequence, the relative effect of flow in enhancing the kinetics becomes more pronounced as the degree of undercooling decreases.

From Fig. 9 (bottom) it also seems that the different curves have a similar shape. It is even possible to shift the data points horizontally to obtain a temperature-invariant mastercurve. Based on a relationship by Liedauer et al. [19] and Eder and Janeschitz-Kriegl [20] for the number of flow-induced nuclei N:

$$N \div \dot{\gamma}^2 t \tag{6}$$

we use the square root of the turbidity half-time under quiescent conditions, $(t_{1/2,q})^{0.5}$, as the horizontal shift factor. In shear-induced crystallization, the small number of quiescent nuclei (being approximately constant versus time) will finally be overruled by the number of shear-induced nuclei, which increases according to Eq. (6). The first observation of a reduction of the turbidity half-time, however, will occur close to the quiescent turbidity half-time $t_{1/2,q}$. It is thus reasonable that a scaling with $\dot{\gamma}^2 t_{1/2,q}$ or $\dot{\gamma}(t_{1/2,q})^{0.5}$ is found. In their work Hadinata et al. [16] used the same shift factor based on the crystallization onset time but only in the range of low shear rates.

The resulting mastercurve for PB0400 is shown in Fig. 10. Both the x-axis and y-axis are now scaled using the turbidity half-time under quiescent conditions. The mastercurve contains data points in the experimental temperature range from 93 °C to 103 °C.

So far we managed to scale the effect of M_W for relatively monodisperse samples. The effect of temperature could also be scaled, but not the effect of shear strain. For the two iPBs with a similar MWD and for the same shear strain, it therefore should be possible to obtain a parameter-invariant mastercurve by combining the proposed scaling laws.

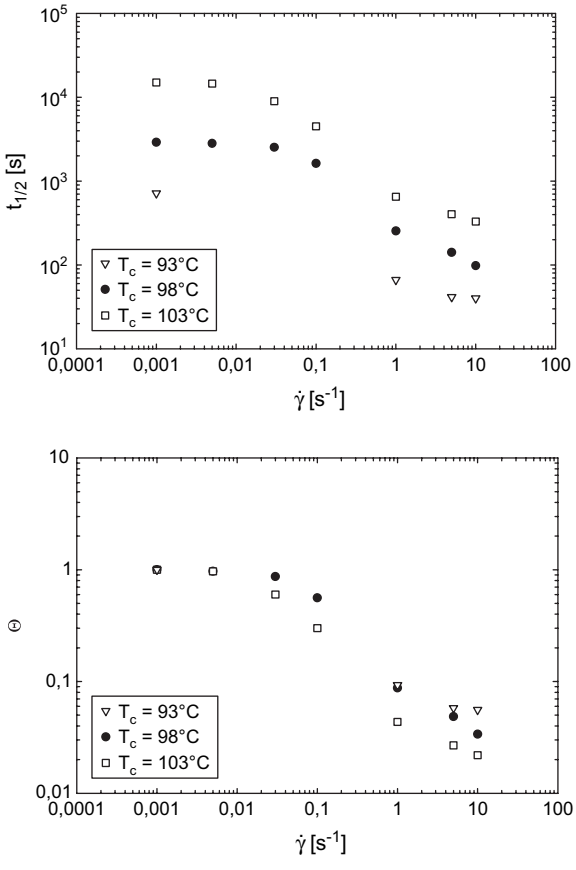

Fig. 9. Turbidity half-time (top) and dimensionless crystallization time (bottom) as a function of shear rate for PB0400 at different crystallization temperatures ($\gamma = 100$).

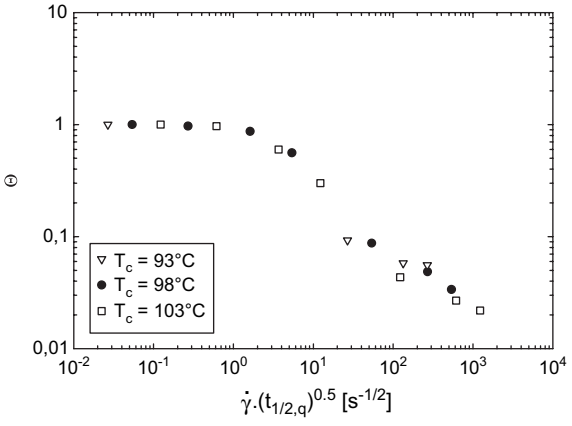

Fig. 10. Dimensionless turbidity half-time as a function of $\dot{\gamma}(t_{1/2,q})^{0.5}$ for PB0400 at different crystallization temperatures ($\gamma = 100$).

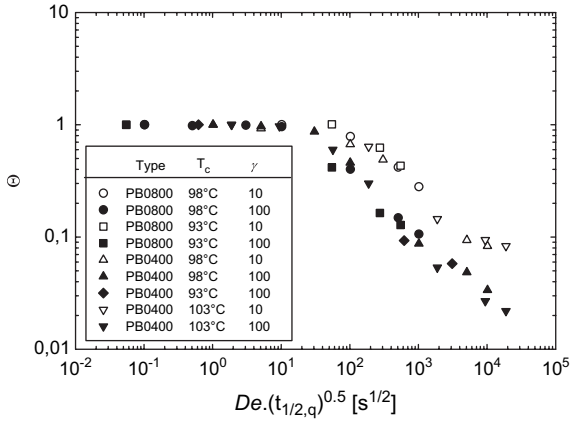

Fig. 11. Grand mastercurves for two types of iPB with a similar MWD and for two different shear strains.

Fig. 11 shows the dimensionless crystallization time as a function of $De\cdot(t_{1/2,q})^{0.5}$. This indeed results in a parameter-invariant 'grand mastercurve'.

3.2.2. Morphology

The growth of the crystalline structures was monitored using optical microscopy. As expected the spherulite radius increases linearly with time until the spherulites impinge. The spherulite growth rate was calculated as the slope of the line approximating the time-evolution of the spherulite radius. In Fig. 12 the growth rates under quiescent conditions at two different crystallization temperatures are plotted as a function of M_W. Despite some scattering it is clear that the growth rate decreases with increasing temperature and is independent of M_W. This could be expected as the growth rate at high crystallization temperatures is determined by the formation of stable nuclei and not so much by diffusion of polymer chains as is the case at low crystallization temperatures (closer to the glass transition temperature). The results from Fig. 12 are in agreement with earlier measurements by Monasse and Haudin [21] and Acierno et al. [14].

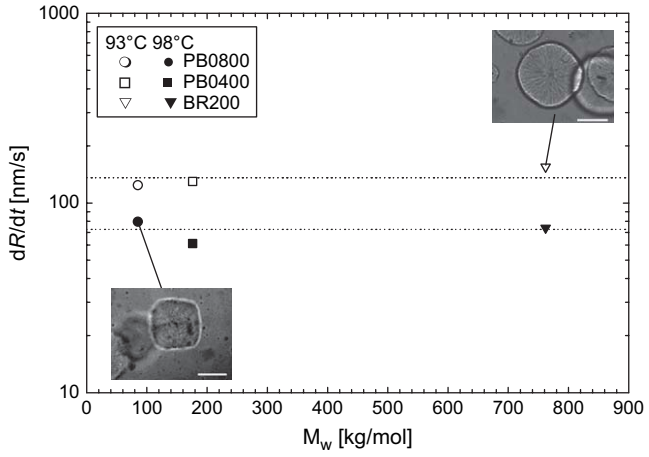

Fig. 12. Growth rates for the three types of iPB at two different crystallization temperatures. The lines indicate the mean values for the two temperatures.

For BR200 and PB0400 the microscopy images showed the expected spherulites, whereas the quiescent crystallization of PB0800 resulted in square-like morphologies, called hedrites. Microscopy images of both structures are inserted in Fig. 12. The reference bar has a length of 100 μm. The occurrence of these two different crystalline structures was reported earlier for similar iPBs by Monasse and Haudin [21], Acierno et al. [14] and Fu et al. [22]. The explanation for this affect proposed by Fu et al. [22] is a change in the crystallization mechanism from folded-chain to chain-extended crystallization which takes place when the crystal thickness d_c gets larger than the radius of gyration R_g of the chains. The observed morphologies were consistent with the phase diagram produced by Acierno et al. [14]. Moreover, Fig. 12 seems to confirm the conclusion by Fu et al. [22] that the change in morphology has no observable effect on the crystal growth rate.

After imposing a shear flow the crystallization becomes much faster than under quiescent conditions. Also, there is a larger number of nuclei, resulting in a finer morphology. This is illustrated in Fig. 13. As can be seen from this figure these effects increase with increasing shear rate. The highest shear rate results in the development of anisotropic rod-like structures that are oriented in the flow direction. This kind of transition with increasing shear rate is typical for polyolefines and was already observed for an isotactic polypropylene by Pogodina et al. [23] and for iPB by Acierno et al. [15]. In later stages the growth of spherulites can also be observed. This phenomenon where, after application of shear flow, anisotropic crystallization is followed by spherulitic overgrowth was first described by Keller and Kolnaar [1] who attributed this effect to the fast relaxing low M_W chains.

As stated earlier in this paper the Deborah number is a good criterion to quantify the effect of shear flow on the crystallization. For very small *De* the quiescent crystallization dynamics dominate. For intermediate *De* there is a relatively large increase in nucleation density but the morphology remains spherulitic. For large *De* the crystalline growth becomes anisotropic and for even more extreme conditions shish-kebabs could form [24]. As a result, high M_W materials will form anisotropic structures more easily because they are characterized by longer relaxation times and thus larger *De* than is the case for low M_W materials under the same shear conditions. This is illustrated in Fig. 14, which clearly shows the effect of M_W on the crystalline morphology: faster crystallization kinetics, a higher nucleation density and development of an anisotropic structure are observed for the higher M_W sample.

4. Conclusions

It has been suggested in this paper that the effect of both M_W and crystallization temperature on the dimensionless crystallization time can be scaled. The effect of shear strain and the MWD was less obvious and more experiments are needed. For the two types of iPB with a similar MWD this resulted in a grand mastercurve. A major significance of this curve is that it can provide a simplified picture of the crystallization

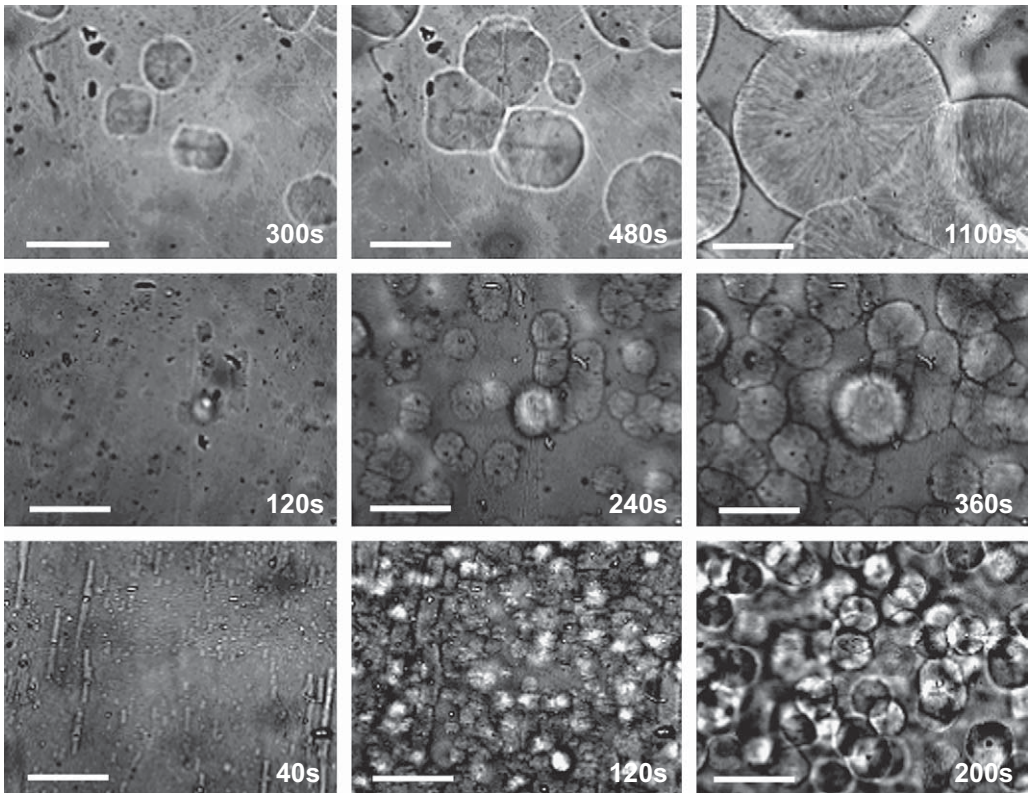

Fig. 13. Effect of shear flow on the morphology of PB0400 crystallizing at 93 °C ($\gamma = 100$); first row: quiescent, second row: 1 s^{-1}, third row: 10 s^{-1}. The reference bar has a length of 100 μm.

kinetics of the polymer sample. It is also useful to investigate the effects of molecular and processing parameters on shear-induced crystallization.

Observations with optical microscopy resulted in information about the crystallite growth rate under quiescent conditions and the crystalline morphology. In a similar way as for the turbidity measurements the effect of the different parameters on the observed transition from an isotropic morphology at low shear rates to an anisotropic structure at high shear rates could be explained in terms of the relaxation behavior of polymer chains. For relatively small *De* only an increase in nucleation density is observed, whereas for large *De* there is a transition from an isotropic to a more anisotropic morphology.

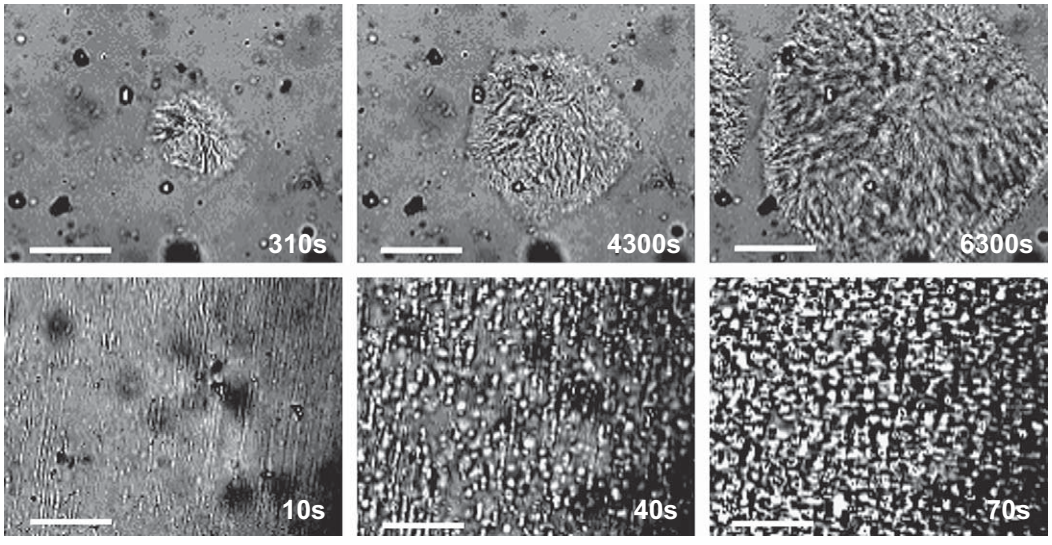

Fig. 14. The effect of M_w on the morphology of iPB crystallizing at 98 °C ($\dot{\gamma} = 1\ s^{-1}$, $\gamma = 10$); first row: PB0800, second row: BR200. The reference bar has a length of 100 μm.

Acknowledgements

The authors wish to thank Dr. H. M. Laun from BASF and Dr. G. Jackers and J. De Clippeleir from Basell Polyolefines for providing the iPB samples.

References

[1] Keller A, Kolnaar HW. Flow induced orientation and structure formation. In: Meijer HEH, editor. Processing of polymers, vol. 18. New York: VCH; 1997. p. 189–268.
[2] Lagasse RR, Maxwell B. Polym Eng Sci 1976;16:189–99.
[3] Tribout C, Monasse B, Haudin JM. Colloid Polym Sci 1996;274:197–208.
[4] Liedauer S, Eder G, Janeschitz-Kriegl H, Jerschow P, Geymayer W, Ingolic E. Int Polym Process 1993;8:236–44.
[5] Jerschow P, Janeschitz-Kriegl H. Int Polym Process 1997;12:72–7.
[6] Kumaraswamy G, Issaian AM, Kornfield JA. Macromolecules 1999;32:7537–47.
[7] Jay F, Monasse B, Haudin JM. J Mater Sci 1999;34:2089–102.
[8] Duplay C, Monasse B, Haudin JM, Costa JL. J Mater Sci 2000;35:6093–103.
[9] Vleeshouwers S, Meijer HEH. Rheol Acta 1996;35:391–9.
[10] Somani RH, Hsiao BS, Nogales A, Srinivas S, Tsou AH, Sics I, et al. Macromolecules 2000;34:5902–9.
[11] Bove L, Nobile MR. Macromol Symp 2002;180:169–80.
[12] Bove L, Nobile MR. Macromol Symp 2002;185:135–47.
[13] Coppola S, Balzano L, Gioffredi E, Maffettone PL, Grizzuti N. Polymer 2004;45:3249–56.
[14] Acierno S, Grizzuti N, Winter HH. Macromolecules 2002;35:5043–8.
[15] Acierno S, Palomba B, Winter HH, Grizzuti N. Rheol Acta 2003;42(3):243–50.
[16] Hadinata C, Gabriel C, Ruellmann M, Laun M. J Rheol 2005;49:327–49.
[17] Ferry JD. Viscoelastic properties of polymers. 3rd ed. New York: Wiley; 1980.
[18] Doi M, Edwards SF. The theory of polymer dynamics. Oxford: Clarendon Press; 1986.
[19] Liedauer S, Eder G, Janeschitz-Kriegl H. Int Polym Process 1995;3:243–50.
[20] Eder G, Janeschitz-Kriegl H. Crystallization. In: Meijer HEH, editor. Materials science and technology, vol. 18. New York: Wiley-VCH; 1997.
[21] Monasse B, Haudin JM. Macromol Symp 1988;20/21:295–302.
[22] Fu Q, Heck B, Strobl G, Thomann Y. Macromolecules 2001;34:2502–11.
[23] Pogodina NV, Lavrenko VP, Srinivas S, Winter HH. Polymer 2001;42:9031–43.
[24] Braun J, Wippel H, Eder G, Janeschitz-Kriegl H. Polym Eng Sci 2003;43:188–203.